Spring 2013

Significance and analysis of milia-like cysts in dermoscopy skin lesion images

Sneha K. Mahajan

Department:

SIGNIFICANCE AND ANALYSIS OF MILIA-LIKE CYSTS IN DERMOSCOPY SKIN LESION IMAGES

by

SNEHA K. MAHAJAN

A THESIS

Presented to the Faculty of the Graduate School of the

MISSOURI UNIVERSITY OF SCIENCE AND TECHNOLOGY

In Partial Fulfillment of the Requirements for the Degree

MASTER OF SCIENCE IN ELECTRICAL ENGINEERING

2013

Approved by

Randy H. Moss, Advisor
R. Joe Stanley
Kurt L. Kosbar

PUBLICATION THESIS OPTION

This thesis consists of the following 3 articles formatted in the accordance with the university specs:

Pages 11-18 Published in Journal of European Academy of Dermatology and Venereology.

Pages 19-28 Accepted as a poster for the International Conference on Vision Theory and Applications (VISAPP 2012).

Pages 29-48 to be submitted to Transactions in Medical Imaging, IEEE 2013.

An introduction section and a conclusions section has been added for purposes normal to thesis writing.

ABSTRACT

Milia-like cysts (MLCs) are dermoscopic structures frequently observed in seborrheic keratoses(SKs), which are the most common type of skin lesions. Diverse appearances of these skin lesions make them difficult to differentiate from melanoma, a deadly type of skin cancer. Classified by size into two main groups, starry MLCs and cloudy MLCs, the presence of these structures in a skin lesion has been known to help differentiate benign lesions from melanoma. Though the presence of cloudy MLCs is not exclusively associated with SKs, they can be a useful tool to differentiate SKs from melanoma. This research study determines the statistical occurrence of MLCs in benign vs. malignant lesions and presents models to differentiate them from the mimics. Various distinct features of these structures such as size, brightness relative to surrounding area, color and shape were used to mark them among the lesions in a training set. A logistic regression model was then used to verify the significant features differentiating these structures from the MLCs and resulted in an area under the receiver operating curve (ROC) of 92.4% for cloudy MLCs and 88.2% for starry MLCs. These models were validated by using a test set.

ACKNOWLEDGMENTS

I would like to express appreciation to my advisor, Dr. Randy Hays Moss, whose expertise, understanding and invaluable opinions have added to my knowledge and success in this graduate program. I value his enormous patience in guiding me through the tough times. I would sincerely like to thank Dr. William V. Stoecker, who has supported me throughout this research and always takes time out from his very busy schedule to continuously guide and supervise me. I thank Viswanaath Subramanian and Sherea Stricklin, whose initial work on this project established the foundation from which I could continue my work. I also wish to thank Dr. R. Joe Stanley for his thoughtful inputs throughout the way. I also would like to express thanks to Dr. Kurt Kosbar, whose course helped me understand all the statistics involved in my research. Also, I would like to express my gratitude to Jason Hagerty who has been a great source of fascinating information and ideas and with whose guidance I was able to view medical imaging with an interesting outlook.

I would also like to thank my family for the overwhelming support they have provided me through my life that motivated me to keep moving on and overcome all the difficulties I faced.

TABLE OF CONTENTS

Page

LIST OF ILLUSTRATIONS

Page

PAPER 1

PAPER 2

PAPER 3

LIST OF TABLES

PAPER 2 Page

PAPER 3

1. INTRODUCTION

In this research, the statistical presence of dermoscopic structures called milia-like cysts in benign seborrheic keratoses vs. malignant melanoma is analyzed to develop models based on selected features via logistic regression to differentiate true MLCs from mimics. Figure 1 shows the starry and cloudy milia-like cysts in a lesion clinically diagnosed as seborrheic keratoses, with, some of the mimics for starry and cloudy milia-like cysts are also marked. This research study will attempt to show that the presence of milia-like cysts in a lesion is an indication that the lesion is benign.

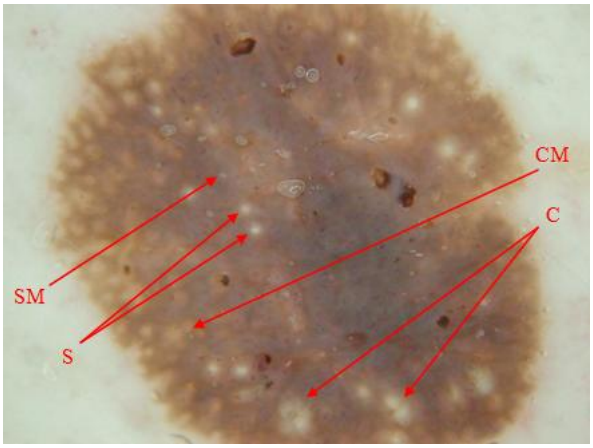

Figure 1: Starry and cloudy milia-like cysts marked as S and C and their mimics marked as SM and CM

To support this hypothesis, this research study presents three papers. The first paper, “Cloudy and Starry Milia-like Cysts: How Well Do They Distinguish Seborrheic Keratoses from Malignant Melanomas?” by Stricklin et al. discusses the two major types of milia-like cysts: starry and cloudy. This paper proposes that the presence of cloudy milia-like cysts is a more specific sign for a lesion being benign as opposed to the presence of starry milia-like cysts. Among the samples collected from various clinics a specificity of 99.1% for presence of cloudy milia-like cysts in seborrheic keratoses vs.

melanoma is observed as opposed to a specificity of 90.1% for presence of starry milia-like cysts.

The next paper, “Template Matching for Detection of Starry Milia-like Cysts in Dermoscopic Images” by Subramanian et al. presents a detailed study and a logistic model to distinguish starry milia-like cysts from their mimics such as scales, skin pores, and small bubbles. These mimics occur in seborrheic keratoses as well as in melanoma. This paper presents a model to distinguish the mimics from true starry milia-like cysts. Various approaches such as template matching and intensity drop profiling have been used.

The next paper, “Two-Stage Template Matching for Detection of Cloudy Milia-like Cysts in Dermoscopic Images of Skin Lesions”, by Mahajan et al. presents an analysis of the cloudy milia-like cyst structures in dermoscopic images of skin lesions. A model generated by logistic regression is presented to make a distinction between mimics such as hypo-pigmented skin networks and the true cloudy milia-like cysts. A two stage template matching approach is utilized to mark locations, and detailed analysis of selected areas follows.

PAPER

I. CLOUDY AND STARRY MILIA-LIKE CYSTS: HOW WELL DO THEY DISTINGUISH SEBORRHEIC KERATOSES FROM MALIGNANT MELANOMAS?

Keywords: Milia-like Cyst, Seborrheic Keratosis, Melanoma

Authors: SM Stricklin, BA; WV Stoecker, MS, MD; MC Oliviero, ARNP; HS Rabinovitz, MD; SK Mahajan, BS

Author Affiliations:

Stoecker & Associates, Rolla, MO (Dr Stoecker and Ms Stricklin); Skin and Cancer Associates, Plantation, Florida (Dr Rabinovitz and Ms Oliviero); Missouri University of Science and Technology (Ms Mahajan)

All correspondence should be sent to:

William V. Stoecker, MS, MD

Stoecker & Associates

1702 East 10th Street

Rolla, MO 65401-4600

Tel: 573-364-0122

Fax: 573-364-0129

Email: wvs@mst.edu

Funding/Support: This publication was made possible by Grant Number SBIR R44 CA-101639-02A2 of the National Institutes of Health (NIH).

ABSTRACT

Seborrheic keratoses are the most common skin lesions known to contain small white or yellow structures called milia-like cysts. Varied appearances can sometimes make it difficult to differentiate benign lesions from malignant lesions such as melanoma, the deadliest form of skin cancer found in humans.

The purpose of this study was to determine the statistical occurrence of milia-like cysts in benign versus malignant lesions.

A medical student with dermoscopy experience and a dermoscopy-naïve observer analyzed 396 contact dermoscopy images of seborrheic keratoses and malignant melanomas for presence of milia-like cysts.

The observers found two different types of milia-like cysts present: large ones described as cloudy and smaller ones described as starry. Starry milia-like cysts were found to be prevalent in both seborrheic keratoses and melanomas. Cloudy milia-like cysts, however, were found to have 99.1% specificity for seborrheic keratoses among a group of seborrheic keratoses and melanomas.

Cloudy milia-like cysts can be a useful tool for differentiating between seborrheic keratoses and melanomas.

1. INTRODUCTION

Milia-like cysts (MLCs) are dermoscopic structures that have been described as "variously sized, white or yellowish, roundish structures."[1] MLCs are "seen in certain pigmented lesions, particularly seborrheic keratoses and congenital melanocytic nevi."[2,3] MLCs have been shown to be useful in distinguishing melanomas from benign lesions.[1,3] In order to characterize those MLCs which can best distinguish melanoma from seborrheic keratoses, DermLite fluid contact dermoscopy (3Gen LLC, San Juan Capistrano, CA) images of 175 seborrheic keratoses and 221 melanomas, of which 128 were melanomas in situ, were analyzed. Two types of MLCs were observed with dermoscopy: starry MLCs and cloudy MLCs (Fig. 1).

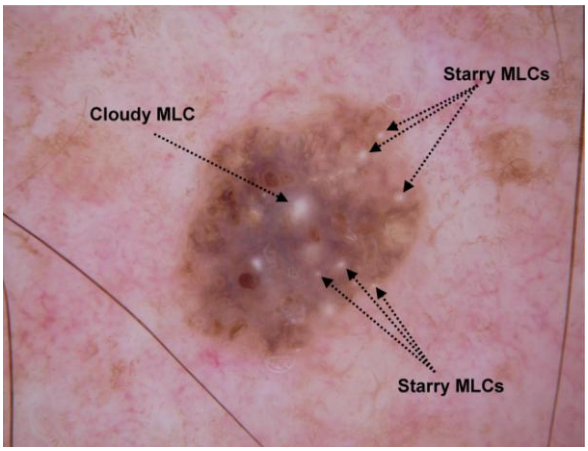

Figure 2: Seborrheic keratosis with a cloudy MLC and multiple starry MLCs.

The starry MLCs are smaller than 1/3mm and often appear like stars on a misty night, with bright centers and variably sharp borders (Fig. 2). They are common in both seborrheic keratoses and congenital nevi, and are sometimes seen in malignant lesions, both melanoma and melanoma in situ (Fig. 3). Cloudy MLCs appear less frequently. They are at least 1/3mm in diameter and they possess a hazy border and an approximately

oval shape that lacks significant irregularities. The cloudy MLCs are more useful in distinguishing seborrheic keratoses from all melanomas (Fig. 4).

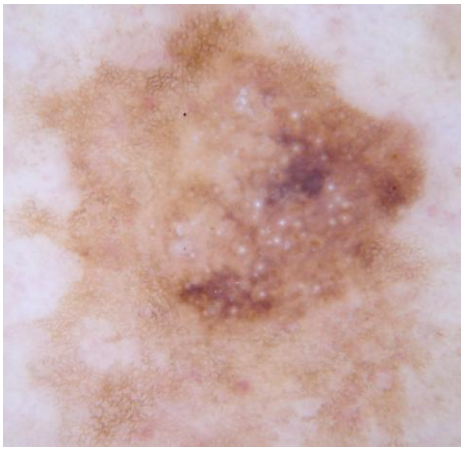

Figure 3: Seborrheic keratosis with multiple starry MLCs.

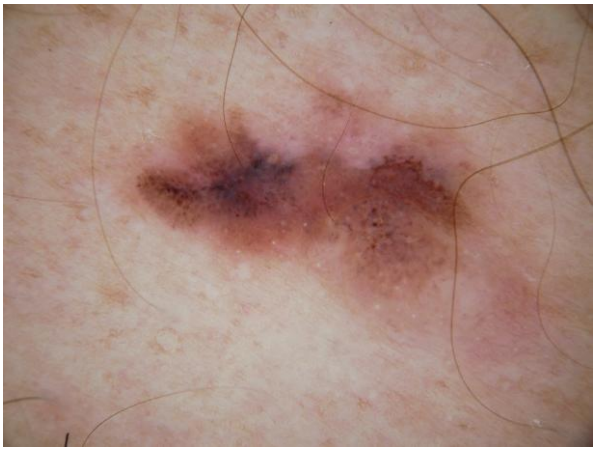

Figure 4: Invasive melanoma 0.63mm thick with multiple starry MLCs, indicating evolution from a congenital nevus.

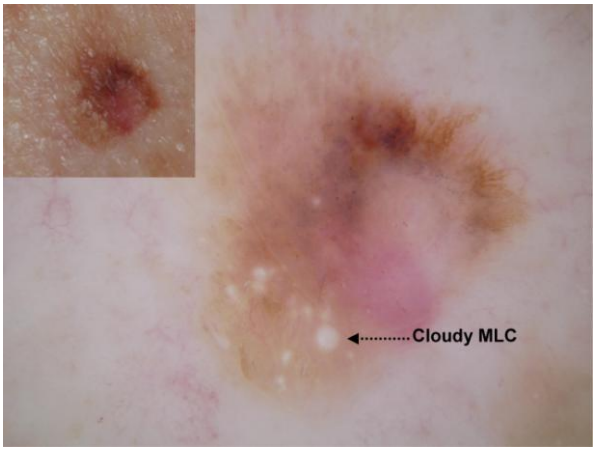

Figure 5: A lesion that clinically resembled a melanoma (inset); the cloudy MLC among multiple starry MLCs suggests a seborrheic keratosis, confirmed with histopathology.

2. METHODS

In order to determine statistically the likelihood of cloudy and starry MLCs appearing in melanomas versus seborrheic keratoses, the 396 images were analyzed for occurrence of each type of MLC. The assessment of MLCs present in each image was scored as follows: starry MLCs, cloudy and starry MLCs, cloudy MLCs or no MLCs. The possibility of bias entering in the study was recognized. An experienced observer would know the diagnosis of a dermoscopy image in most cases, and this could influence the assignment of the types of MLCs present. A naïve observer, unaware of the project's hypothesis, with no previous dermoscopy background and therefore no experience in distinguishing melanomas from seborrheic keratoses was trained in recognizing MLCs. Each image was scored independently by the naïve observer (SKM) and by a trained observer with knowledge of the different diagnoses (SMS).

The most difficult objective in the study was separating MLCs from competing structures such as small areas of keratin scale, bubbles from the contact dermoscopy fluid interface, and tiny pigment network holes. Small keratin scales, the most problematic competing structures, were distinguished from MLCs by their irregular borders, noise within the area, and asymmetry. The irregular borders and the noise were determined as clearly as possible by zooming in on images. The resolution of 1024 x 768 pixels allowed clear differentiation of MLCs from scales. Gel bubbles tend to be more gray or transparent in appearance and generally have a smaller circle within the outer bubble ring. Difficult bubbles more closely resembling MLCs were tested by comparing the image with another type of contact dermoscopy image taken the same day. If the area in question was not in the same spot in both images, then it was determined to be a bubble.

Tiny pigment network holes are differentiated from MLCs by a ring of pigment surrounding lighter skin coloring. For cloudy MLCs, the size was confirmed by analysis of the fully zoomed DermLite fluid images that are 9mm across. A scale was then calibrated to measure 1/3mm in relation to the image. For images that had been zoomed out, there was a scale in millimeters on the image. This scale was then used to calibrate 1/3mm in relation to these images

3. RESULTS

The two observers disagreed on 10.9% of the images but were able to reduce the disagreement on all but approximately 5%. The remaining differing assessments were arbitrated by an experienced dermoscopist (WVS). After complete consensus was achieved by the two observers and a dermatologist, the odds ratio, sensitivity and specificity was calculated for both starry and cloudy MLCs.[4] For starry MLCs, our analysis showed an odds ratio of 8.0 (4.7-13.7) with a 90.5% sensitivity and 45.7% specificity for a diagnosis of seborrheic keratosis versus all melanomas. An odds ratio of 27.4 (7.2-104.4) with 20.0% sensitivity and 99.1% specificity was obtained for seborrheic keratoses having a cloudy MLC versus melanomas. Odds ratios, usually denoting the odds of a malignant diagnosis for a given sign, are given here as the odds of a benign diagnosis for the given sign.

4. DISCUSSION

Due to incomplete separation of malignant from benign lesions, especially for the more common starry MLCs, one model for discriminating amelanotic and hypomelanotic melanomas developed by Menzies et. al includes the number of MLCs: when there are three or more MLCs present, the model uses this feature to predict a benign lesion.[3] No size distinction was given for MLCs in the three-or-greater model.[3] If there is no discrimination by size, and tiny (starry) MLCs are considered equivalent to large (cloudy) MLCs, melanomas with a congenital nevus precursor (Figure 3) will be counted benign. The Menzies study included only amelanotic/hypomelanotic melanomas and did not separate starry and cloudy MLCs, therefore findings of that study are not strictly comparable to our findings.

In our experience, cloudy MLCs are rarely seen in melanomas, as only 2 of 221 lesions had cloudy MLCs. Cloudy MLCs appear to be more useful than starry MLCs as a "benign sign." However, as cloudy MLCs were not found to be pathognomonic, other factors present in the clinical and dermoscopy presentation should always be considered alongside the cloudy MLC sign.

ACKNOWLEDGMENTS

Rhett Drugge, MD and Lindall Perry, MD supplied images used in the statistical analysis.

REFERENCES

[1] Argenziano G, Soyer HP, Chimenti S, et al. Dermoscopy of pigmented skin lesions: results of a consensus meeting via the Internet. J Am Acad Dermatol. 2003; **48**:679-93.

[2] Arch Dermatol. 2007 Aug;143(8):1007-14.

[3] Age- and site-specific variation in the dermoscopic patterns of congenital melanocytic nevi: an aid to accurate classification and assessment of melanocytic nevi.

[4] Changchien L, Dusza SW, Agero AL, Korzenko AJ, Braun RP, Sachs D, Usman MH, Halpern AC, Marghoob A

[5] Berk DR, Bayliss SJ. Milia: a review and classification. J Am Acad Dermatol. 2008; **59**:1050-63.

[6] Menzies SW, Kreusch J, Byth K, et al. Dermoscopic evaluation of amelanotic and hypomelanotic melanoma. Arch Dermatol. 2008;**144**:1120-7.

[7] John C. Pezzullo. "2-way Contingency Table Analysis.". 2010. Available at: http://statpages.org/ctab2x2.html (last accessed 6 June 2010).

II. TEMPLATE MATCHING FOR DETECTION OF STARRY MILIA-LIKE CYSTS IN DERMOSCOPIC IMAGES

Viswanaath Subramanian[1], Randy H. Moss[1], Ryan K. Rader[2], Sneha K. Mahajan[1], William V. Stoecker[1,2]

[1]*Department of Electrical and Computer Engineering, Missouri University of Science & Technology,*

141 Emerson Electric Co. Hall, Rolla, MO, USA

[2]*Stoecker & Associates, 10101 Stoltz Drive, Rolla, MO, USA*

{vsgzd, rhm, rkrc5b, skmdm2, wvs}@mst.edu

Keywords: Pattern Analysis; Image Processing; Object Detection; Template Matching; Seborrheic Keratoses; Milia-like Cysts

ABSTRACT:

Early detection of melanoma by magnified visible-light imaging (dermoscopy) is hindered by lesions with similar dermoscopic appearance. Automatic discrimination of melanoma from mimics could allow detection of melanoma at an earlier stage. The most common of these mimics are seborrheic keratoses, which have distinctive bright structures: starry milia-like cysts (MLCs). We report here discrimination of melanoma from seborrheic keratoses by features extracted from MLCs. After pre-processing, 2D template matching is optimized with respect to template size, histogram pre-processing, and 2D statistical techniques. Other extracted features include brightness, both absolute and relative to the star surround, shape features calculated at boundary and 1D brightness rise-time. Logistic regression analysis was applied and the features retained in the final model were 1D rise time, 2D first correlation coefficient, star size, and relative star

brightness. The methods reported here allow optimization of MLC features found by 2D template correlation. This research confirms the importance of structure neighborhoods in medical imaging.

1. INTRODUCTION

Milia-like cysts (MLCs) are dermoscopic structures that are mostly white or yellowish in color, vary in size, and are most commonly seen in seborrheic keratoses. Their presence in benign lesions makes MLCs an attractive feature to distinguish

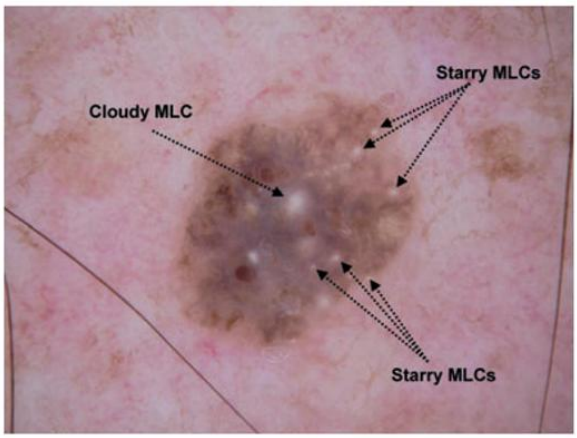

Figure 6: Seborrheic keratosis with a cloudy MLC and multiple starry MLCs (Stricklin et al., 2011).

melanomas from benign lesions (Argenziano et al, 2003; Braun et al, 2002; Menzies et al, 2008; Stricklin et al, 2011). MLCs are classified as either starry or cloudy (Figure 6). Starry MLCs are less than 1/3 mm in diameter, round and often appear like "stars on a misty night" (Stricklin, 2011). Cloudy MLCs are greater than 1/3 mm in diameter, and have a cloudy, less sharp, oval border.

Starry and cloudy MLCs have certain characteristics, discussed in Section 4, which can be used to separate them from competing structures such as small areas of keratin scale, bubbles from the contact dermoscopy fluid interface, and tiny pigment pores. Stricklin et al. found that starry MLCs had 90.5% sensitivity and 45.7% specificity for seborrheic keratosis (Stricklin et al., 2011). Since starry MLCs are mostly white or yellowish in color, the most important factor to consider is the intensity of the area of the

starry MLC in the lesion image. Skin lesions can be varied in color, such as pink, yellow, brown or black, all with differing intensities. Independent of the color within the lesion, the size and shape of starry milia-like cysts do not change.

2. PRE-PROCESSING OF IMAGES

2.1 DATA SETS AND IMAGES USED

The image set consisted of 66 seborrheic keratoses and 34 melanomas acquired in the course of the study NIH CA153927-02A2 which had MLC or MLC-mimicking structures. The Phelps County Regional Medical Center Institutional Review Board, Rolla, Missouri USA approved this research, and informed consent was obtained from all participants. Contact, non-polarized dermoscopy images were taken with a Sony DSC-W70 digital camera and 3Gen DermLite DL2 dermatoscope (3Gen LLC, San Juan Capistrano, CA). Images were reduced to 1024×768 resolution and retained full, 24-bit color.

2.2 USE OF BLUE PLANE

The blue plane is chosen from the other primary color planes for contrast detection in MLCs, as Lee also used for segmenting lesion borders (Lee, 2001).

2.3 FORMATION AND PROCESSING OF LESION AREA

The border contour outlining the lesion area was manually drawn and verified by a dermatologist (W.V.S.) using a second-order spline technique, as in previous studies (Cheng et al, 2008; Dalal et al, 2011); (Stoecker et al, 2005).

Bubbles that result from the contact dermoscopy fluid interface can mimic starry MLCs. To prevent this, a bubble mask was generated from an automated bubble detection program which detected high intensity and high gradient areas and was applied to subtract bubbles from the image before analysis occurs. Manual removal of hairs was performed for images containing hairs.

3. CANDIDATE STAR SELECTION

3.1 SELECTION OF CANDIDATE PIXELS BY APPLYING BLOCK-BY-BLOCK SELECTION OF MAXIMUM INTENSITY PIXEL VALUE

To reduce the computational load by selecting only the most promising candidate stars (starry MLCs), the lesion area is divided into 13×13 pixel blocks. The brightest pixel in each 13×13 block is chosen as the center for a candidate star.

3.2 APPLICATION OF LESION AREA MEAN AS THRESHOLD

Since starry MLCs are brighter than their surroundings, the number of candidate starry MLCs can be additionally reduced using a mean threshold. First, the mean intensity value of the entire lesion area is calculated. If the value of the individual pixel selected in each 13×13 window is greater than the mean intensity value, that pixel meets the criteria for further processing as a candidate star. In order to avoid "noisy" pixels such as "salt and pepper" noise, an averaging filter with equal weights was applied using a 3x3 neighborhood function centered on each candidate pixel before comparing the mean value against the mean of the lesion area.

The mean threshold was decreased to 0.85 times the mean intensity value, as there were instances when the threshold was the mean intensity value where stars were lost if they resided in dark areas.

3.3 REJECTING DUPLICATE CANDIDATES

We then consider the situation of starry MLCs whose areas are larger than 13×13 pixels. By applying block-by-block analysis of maximum intensity pixel values, two or more pixels of the same starry MLC could be selected if a single starry MLC was located in more than one 13×13 block. If two candidate pixels occur in the same 13×13 block,

the pixel with the highest intensity is designated as the candidate pixel and all other pixels are discarded. These discarded pixels will not be further considered as candidates for being a starry MLC.

4. CHARACTERISTICS OF STARRY MLCS

Starry MLCs have bright centers and reduced intensity when radially expanded. Initially, the stars were considered to be circular, so row vector techniques were applied to check the consistency of intensity drops across the central row within a starry MLC. When the center row containing the central pixel is plotted, a peak at the center is obtained as shown in Figure 7. The shape of this graph, with respect to features such as the slope of the rise and fall of intensity and the difference in intensity between the peak and the surrounding, can be used to statistically define a starry MLC.

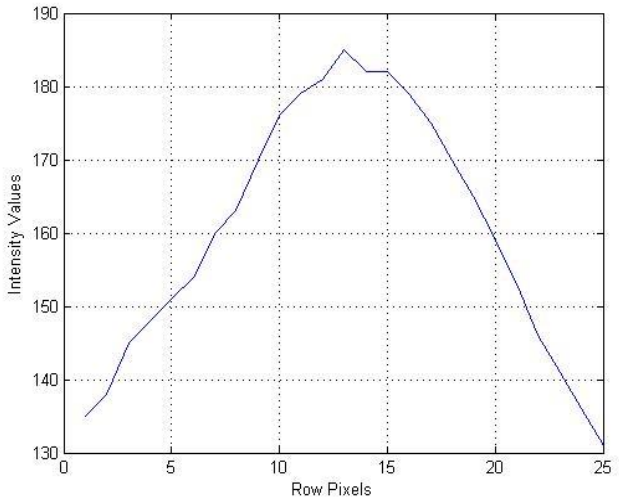

Figure 7: A graph of intensity values plotted across a starry MLC through the center pixel.

The slope of the rise and fall of intensity are calculated from the outermost pixels of the center pixel along the center row. The standard deviation and variance are determined over the whole starry MLC area. To maintain consistency between starry MLCs of varied size, only the central area of 11×11 pixels of starry MLC candidates

were selected for calculations. The mean intensity is calculated over the central 11×11 pixel area. To define the star and its surrounding, we consider two concentric circles where the star is the inner square centered on the candidate pixel where each side of the square is of length Z pixels and the surround is three pixels wide (making each side of the outer square Z+6 pixels long). The mean of the surround is calculated over this 3-pixel-wide "ring". The difference between the mean of the star and the mean of its surround is also calculated according to the size of the starry MLC (determination of size described in Section 5.2). The size of the surround is fixed as a "ring" with a width of three pixels.

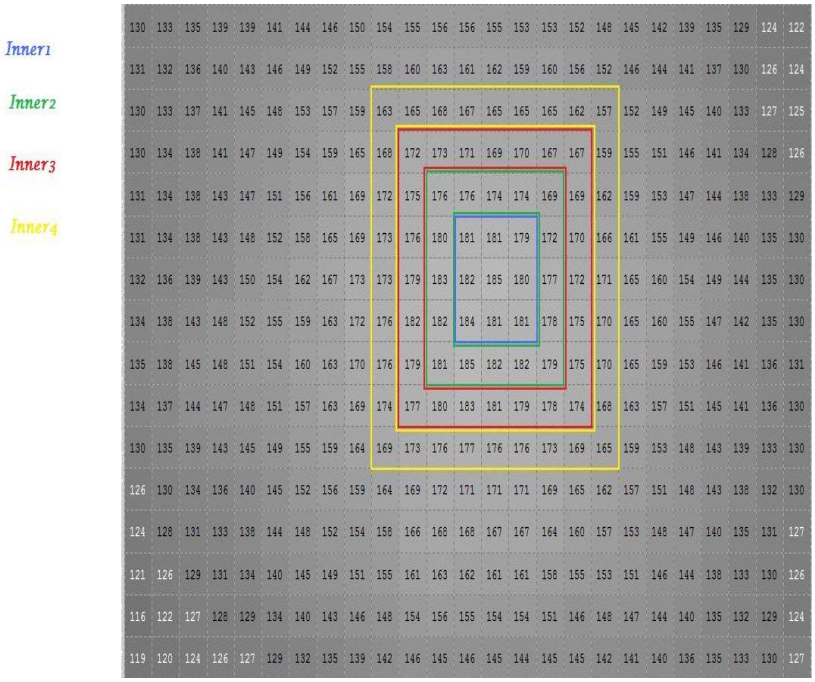

Figure 8: Difference between the mean of concentric squares.

From each candidate star, we collected the following statistics using the row vector technique.

1. Rise Time: The rate of intensity change from the surrounding to the maximum central intensity value

2. Fall Time: The rate of intensity change from the peak central intensity value to the surrounding
3. Standard deviation
4. Variance
5. Difference between the mean intensity value of the star and the surround

To get more details about the star, the difference in intensity between each consecutive concentric ring around the central pixel was calculated. Figure 8 displays an enlarged grayscale image of a starry MLC showing the pixel intensity values. The mean of each ring is calculated and the difference between the mean intensities of consecutive rings is calculated. Each ring is given a name (e.g. inner1, inner2, inner3). Hence, (inner1-inner2) is the difference in the mean of the innermost ring and the second-most ring.

5. TEMPLATE MATCHING USING CORRELATION COEFFICIENTS

The row vector method aided in the identification of the starry MLCs. However, numerous false positives were also detected. To remove those starry MLC mimics, the candidate stars were correlated with a star template to narrow down the number of candidates.

5.1 CORRELATION COEFFICIENT AND ITS SIGNIFICANCE

Correlation has been used extensively for template matching. Consider *f*(x,y) to be an image consisting of different objects or regions. To check whether *f* contains a particular object of interest, let *w*(x,y) be that object. If object *w* is present in *f*, the correlation will be maximized at the location where *w* finds a correspondence in *f*. Matching is performed using the correlation coefficient which is defined as follows:

$$\gamma(x,y) = \frac{\sum_s \sum_t [f(s,t) - \bar{f}(s,t)]\,[w(x+s,y+t) - \bar{w}]}{\{\sum_s \sum_t [f(s,t) - \bar{f}(s,t)]^2 \sum_s \sum_t [w(x+s,y+t) - \bar{w}]^2\}^{1/2}}$$

where x = 0, 1, 2, 3 . . ., M-1, y = 0, 1, 2 . . ., N-1, M×N is the size of *f*, $\bar{w}$ is the mean value of pixels in *w* and $\bar{f}$ is the mean value of the region that is coincident with the current location of *w*. All summations are taken over the coordinates common to both *f* and *w*. The calculated correlation coefficient γ(x,y) is scaled such that the maximum value is 1 and the minimum value is -1. The correlation coefficient is independent of amplitude changes in *f* and *w* (Gonzalez, 2002).

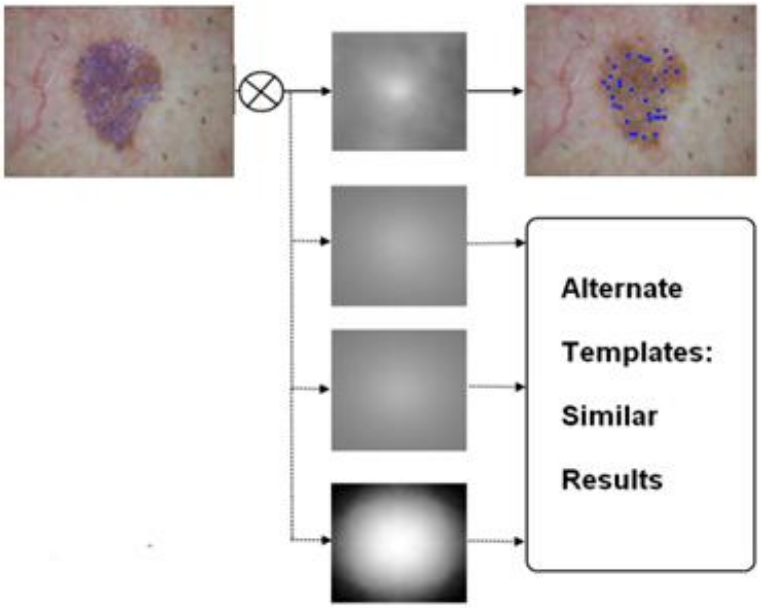

Figure 9: Original template candidates are correlated with 4 unique templates, from top to bottom—star template from actual lesion area, ideal averaged star template, ideal averaged and rotated star template, and histogram-equalized and rotated averaged star template. Similar results are obtained with all templates.

If the candidate star has a similar shape to the star template, the correlation coefficient will be close to 1. However, if we correlate two objects of different shapes, the correlation coefficient will be closer to 0. A threshold was chosen by dividing a range of coefficient values from 0.7 to 1 into nine sections, and selecting the coefficient value with the maximum possible number of candidates without surpassing 50 stars.

5.2 CORRELATION WITH DIFFERENT STAR TEMPLATES

The size of starry MLCs can range from 11 to 25 pixels in diameter, therefore each candidate star was correlated with three star templates of sizes: 11×11, 17×17, and 23×23. The template with the highest correlation coefficient for that star was selected.

The star templates were designed to best resemble the features of an ideal star. Five different options were attempted and analyzed.

1. A star template was selected which had the most ideal characteristics from starry MLCs in our images.
2. A synthetic star template was created which incorporated the intensity drops, standard deviance, and variance seen in true starry MLCs.
3. The intensity values of all the starry MLCs of the same size from a set of images were averaged.
4. The average star template in Option 3 was rotated by multiples of 90° and the average of the orientations was calculated to reduce the effect of different orientations of starry MLCs.
5. Contrast enhancement was applied on the averaged rotated star template to emphasize the decrease in intensity with radial expansion.

Out of the above five star templates, the synthetic star template of Option 2 yielded good results for only certain starry MLCs. Creating synthetic star templates *de novo* with available data was impractical and error-prone; therefore this method was discontinued.

Analysis showed the averaged star and rotated averaged star templates had similar results. Figure 9 shows the result of correlating the candidate stars with the averaged and rotated template; one of four outputs is shown. Each template yielded slightly differing numbers of candidate stars, but always detected the true starry MLCs.

In a small number of cases, the output from the equalized star template varied slightly from the other three star templates, leading to a difference in the number of candidate starry MLCs selected for further analysis.

5.3 APPLICATION OF RANGE AS A THRESHOLD

All starry MLCs have a bright pixel at the center and a decrease in intensity with radial expansion. However, the rate of decrease is not constant in stars as their size can vary between 11 and 25 pixels in diameter. To provide a more consistent method of discrimination, the difference between the maximum and the minimum pixel intensity (i.e. range) was calculated for the 11×11 center of the star. Since skin pores have similar characteristics to starry MLCs, but a low rate of intensity change comparatively, this particular parameter can aid in differentiating true starry MLCs from pores.

From 66 images of seborrheic keratoses, the data regarding the relative variation in pixel intensities in star centers were calculated. This method retained almost all of the true starry MLCs for further processing. The range of pixel intensity in the 11×11 star center, given as a fraction of maximum intensity, are 0.14, 0.075 and 0.03 for star sizes 11, 17 and 23 respectively.

As can be seen from Figure 10, the image that was obtained after the first correlation had 34 candidate stars, whereas the image that was obtained after applying the range threshold for the 11×11 center of the star had only 10 candidate pixels, including all four true starry MLCs in the image. The range threshold was applied to all 100 images (66 images of seborrheic keratoses and 34 images of malignant melanoma) in the training set and it was found that less than 5% of the true starry MLCs were rejected.

6. CANDIDATE STAR SHAPE ANALYSIS

6.1 SHAPE OF THE STARRY MLC

The drop in the intensity values with a radial outwards progression was not constant for all starry MLCs. Additionally, the rate at which the intensity values decreased was not constant in all directions from the center of MLC. These findings can help determine the shape of the star.

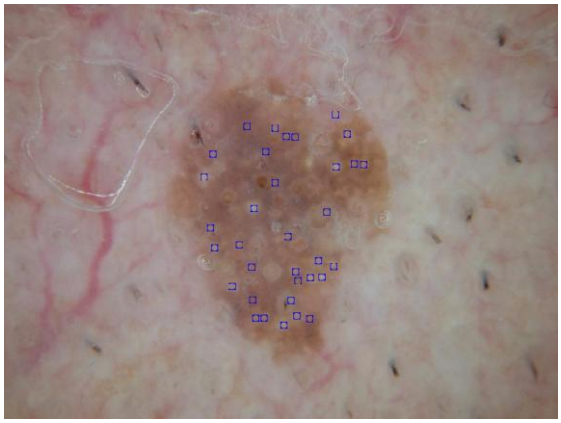

Figure 10: Original image after correlating with star template.

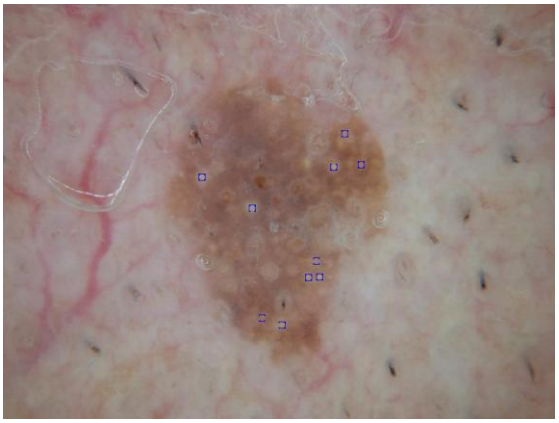

Figure 11: Image after applying the difference between the maximum and minimum pixel intensity value as threshold.

To find the shape, the candidate star was smoothed using a 3×3 mean filter by a sliding neighborhood operation, providing a more constant rate of intensity drop. Both the smooth star template and histogram equalization were used to find the shape of the star.

Once we obtain a smooth star template, depending upon the maximum and minimum intensity of pixel values in the star template, a closed figure is obtained which represents a rough approximation of the shape of the star. The initial shape of the star is a set of points whose intensity values are within ±10% of the average intensity of the smoothed version of the star template. The closed figure is then processed to obtain a single-pixel-wide boundary.

Using this method, the initial shape of the star that is formed is not always a closed figure, when the actual size of the candidate star is greater than the assumed size from the correlation coefficient values. The single-pixel-wide boundary of the star may be incomplete and cannot be fully filled. To solve this problem, a larger size template for the star candidate was considered. The star can be determined as complete or incomplete by calculating its roundness:

$$Roundness = \frac{Perimeter^2}{4\pi \times Area}$$

The perimeter of the object is constant, whereas the area of the object will differ drastically. If the shape of the star is not filled completely:

$$(\text{Perimeter}^2) / (4\pi \times \text{area}) >> 1$$

Whereas if the shape of the star is filled,

$$(\text{Perimeter}^2) / (4\pi \times \text{area}) \approx 1$$

It is therefore straightforward to determine if the shape of the star is filled. If the shape of the star is still incomplete after using a larger template, we presume that the star candidate is a mimic.

Solidity was also used to check whether the shape of the star is filled. A convex hull is the smallest convex polygon that can contain the entire region of the filled shape of the star. Solidity, *S*, specifies the fraction of pixels in the convex hull that are also in the filled shape of star (MATLAB, 2009):

$$S = \frac{A}{A_c}$$

where,

A = Area of the filled shape of star

A_c = Area of convex hull

For a true starry MLC, solidity will be close to one, whereas solidity for a starry MLC mimic will be closer to zero.

True starry MLCs and mimics of starry MLCs can be differentiated using the shape of the star. For true starry MLCs, the shape of the star will be complete and its solidity value will be close to one. The shape of the star for mimics such as keratin scales, skin pores, and bubbles can exist as either complete, closely mimicking true starry

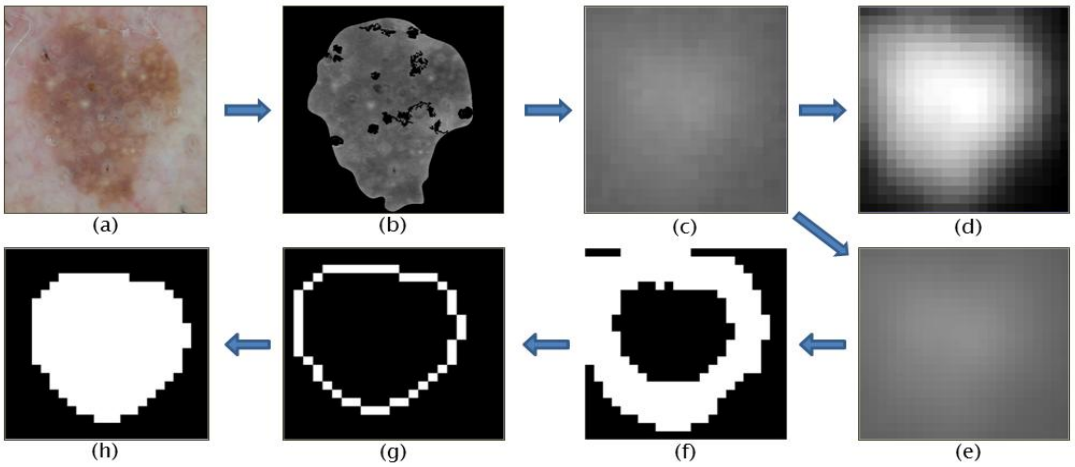

Figure 12: Formation of shape of the star for a true starry MLC. (a) Original image – Seborrheic Keratosis. (b) Lesion and bubble masks applied on blue plane. (c) Enlarged version of a starry MLC. (d) Histogram equalized starry MLC. (e) Enlarged version of smoothed starry MLC. (f) Initial shape of the star. (g) Thinned one pixel width shape of the star. (h) Final filled shape of the star shifted to the center.

MLCs, else the shape of the star will be incomplete or have tail-like structures, resulting in a solidity closer to zero. The process of developing the shape of the star for a true starry MLC is explained with diagrams in Figure 12, as well for mimics in Figure 13.

6.2 SECOND CORRELATION WITH SHAPE OF THE STAR

Once the shape is determined, a new ideal binary star template is created for those measurements. If we assume the shape of the star is elliptical in nature, an elliptical binary star template whose major axis, minor axis, and orientation are equivalent to the shape of the star was constructed.

The original star candidate is correlated with the created ideal star template to determine if the filled shape of the star is a true starry MLC. Since the size of the star is small, i.e. in the range of 11×11 pixels, the correlation coefficient may vary immensely even for small changes in the shape of the star. To overcome this problem, both the filled

shape of the star and the star template formed are equally scaled, then correlated. The scaling factor is different for different sizes of the candidate star: six for 11×11, four for 17×17, and three for 23×23. The scaling factors were chosen so that the scaled template is almost equal irrespective of the actual size of the star candidate. The correlation coefficients in both scaled and un-scaled cases were found to be approximately equivalent.

6.3 CORRELATION WITH A HISTOGRAM EQUALIZED STAR TEMPLATE

The number of mimics wrongly identified as starry MLCs were reduced using the various methods described in the previous sections. Skin pores have a similar template—bright center and radial drop, making these difficult mimics of starry MLCs. However, the rate of drop in intensity is slightly less for skin pores than for starry MLCs. This characteristic is not captured when the various parameters like fall time, rise time, etc., are calculated because the difference is very small. To make this difference visible, the candidate star is histogram equalized to enhance its contrast, then correlated with an equalized ideal rotated averaging star template.

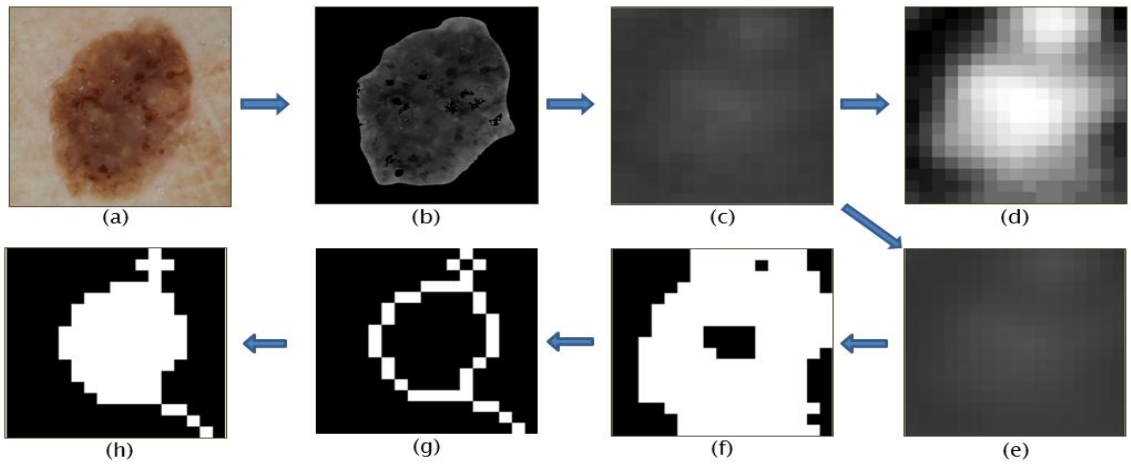

Figure 13: Formation of shape of the star for a mimic of a starry MLC. (a) Original image – Seborrheic Keratosis. (b) Lesion and bubble mask applied on blue plane. (c) Enlarged version of a starry MLC mimic. (d) Histogram equalized starry MLC mimic. (e) Enlarged version of smoothed star mimic. (f) Initial shape of the star. (g) Thinned – one pixel width shape of the star. (h) Final filled shape of the star of starry MLC mimic having tail like structure.

7. MLC ANALYSIS METHODS

The 33 parameters for each candidate starry MLC are as follows, indexed by the stored coordinates for the center of the candidate star:

7.1 FROM THE ORIGINAL STAR CANDIDATE:

After determining the size of the star which can either be 11 or 17 or 23 pixels in diameter, the surround of the star is a ring having a thickness of three pixels wide whose inner radius is the same as the radius of the star. The mean intensity of the star and the surround are calculated by taking the average of all the pixel values in the star and in the surround, respectively.

7.2 FROM THE ORIGINAL IMAGE, THE FOLLOWING DATA IS STORED

1. Center pixel intensity of the candidate star.

7.3 FROM CORRELATING THE CANDIDATE STAR WITH A STAR TEMPLATE

2. Correlation coefficient: The maximum coefficient from correlating the candidate star with three differently sized ideal star templates.
3. Size of star based on best-fit star template.
4. Differences between the intensity values of adjacent rings around the center pixel of the candidate star of different radii ranging from 1 to 5 (four parameters).
5. Rise time and fall time which gives the rate of change of intensity values.
6. Mean of the actual size of star (after choosing size template with highest correlation).
7. Mean of the actual size of surround.

8. Difference between the mean of the star and mean of the surround
9. Standard deviation of the star.
10. Variance of the star.
11. Rise time and the fall time for the 11×11center of the star.
12. Mean of the 11×11 center of the star.
13. Mean of the surrounding of the 11×11 center.
14. Difference between the mean of the star and mean of the surround for the 11×11 star center.
15. Standard deviation of only the 11×11 center of the star.
16. Variance of the 11×11 center.
17. Difference between highest and lowest point in the 11×11 center.

7.4 PARAMETERS CALCULATED FROM THE STAR SHAPE

18. Area: The number of pixels in the region.
19. Perimeter: The distance in pixels around the boundary of the region.
20. Centroid: Specifies the x-coordinate and the y-coordinate of the center of mass of the region as a two-element vector.
21. Major axis is calculated using the MATLAB® 'MajorAxisLength' in 'regionprops', displaying the pixel value of the ellipse major axis whose second central moments are equivalent to that of the region.
22. Minor axis: Calculated similarly as major axis.
23. Equivalent Diameter: The diameter of a circle whose area is the same as the region.
24. Orientation: Angle between the x-axis and the major axis.

25. Eccentricity: Ratio of the distance between the foci and the major axis length of the ellipse. Eccentricity value is always between zero and one.
26. Solidity: Percentage of pixels in the convex hull that is also present in the region. Convex hull specifies the smallest convex polygon that can contain the complete region.
27. $$Roundness = \frac{Perimeter^2}{4\pi \times Area}$$
28. Major axis / Equivalent diameter.
29. Area of the star is filled completely or not.
30. Shape of the star is circular or elliptical. Shape is considered elliptical if the difference between major and minor axes is more than 2 pixels.

7.5 FROM CORRELATING THE SHAPE OF THE STAR WITH A SHAPE OF THE STAR TEMPLATE

31. Second correlation coefficient for the scaled shape of star.
32. Second correlation coefficient for the un-scaled shape of star.
33. Correlation coefficient of the histogram equalized candidate starry MLC with a histogram equalized star template.

8. RESULTS

All parameters discussed in Section 7 were analyzed by the Statistical Analysis System (SAS; SAS Institute, Cary, NC). The total number of candidate pixels analyzed by logistic regression was 1005 candidates from the seborrheic keratosis images and 473 candidates from the melanoma images. The most significant features determined by logistic regression (Table I) and the corresponding receiver operating curve (Figure 14) are displayed. Note that the area under the ROC curve is 88.2%.

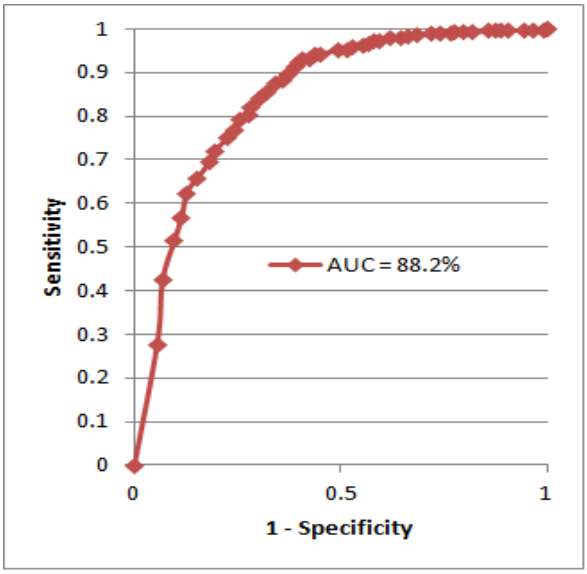

Figure 14: Receiver Operating Characteristic

Table 1: Most significant features from logistic regression model

Parameter	**Chi-Square**	**Pr > ChiSq**
Size of the star	24.6856	< .0001
First Correlation Coefficient	29.1704	< .0001
Intensity difference between mean of star and surround	25.5965	< .0001
Mean of 11x11 star	8.6837	0.0032
Variance of 11x11 star	10.0570	0.0015
Rise time of 11x11 star	30.8251	< .0001
Second correlation coefficient scaled	11.1896	< .0008
Equalized correlation coefficient	29.2425	< .0001

9. CONCLUSION

This research was conducted to classify a lesion based on the presence of multiple starry milia-like cysts, indicating seborrheic keratosis. To identify a certain object, template matching was used to correlate: 1) the candidate star with an ideal star template, 2) the binary shape of the star with the generated ideal shape of the star and 3) the histogram equalized candidate star with the histogram equalized ideal star template. Characteristics of starry MLCs, such as drop in intensity, size and shape, mean and variance, etc., were studied to create star templates for template matching. Of the parameters discussed in Section 7, the three most significant were: 1) the size of the star, 2) the correlation coefficient between the candidate star and an ideal star template, and 3) the difference between the star and the surround. The accuracy and the area under the receiver operating characteristic curve show that the algorithm presented here can identify most starry MLCs.

10. FUTURE WORK

Using SAS logistic regression analysis, a candidate star can be correctly identified as a true starry MLC with a maximum of 86% accuracy, and an area under the curve for the receiver operating characteristic of 88.2%. This accuracy may be increased if the following steps are implemented:

1. Milia-like cysts are classified as starry MLCs or cloudy MLCs depending upon the size of the MLC. It was decided that the MLCs whose diameters are greater than 30 pixels wide, corresponding to the limits advocated by Stricklin et al., will be classified as cloudy MLCs. Correspondingly, all the MLCs whose diameter is less than 30 pixels wide are classified as starry MLCs. In this research project, the size of the star was varied from 11 to 23 in steps of six. Hence, three different sizes of star having diameter 11, 17 and 23 were considered. The accuracy could increase if more steps in the range 5 to 31 pixels in diameter are considered.
2. The characteristics of the MLC mimics such as pores, bubbles and scales can be calculated and used to aid in differentiation of MLC and mimics.
3. Bubbles account for a fraction of the false positives that were identified as starry MLCs. The bubble mask removed a majority of the bubbles, however progress can be made to optimize this mask.
4. Logistic regression analysis used 66 images of seborrheic keratoses and 34 images of melanoma. The classification accuracy can be increased by training SAS with more images.

5. Analysis concentrated only on the blue plane of the image. The blue plane yields an overall accuracy equal to 86%; however incorporating the other color planes may improve the accuracy of the results.
6. A square template was used for correlation. However, a circular template can be used. Since starry MLCs are mostly circular in shape, a circular template might yield a higher correlation versus a square template.

REFERENCES

[1] Argenziano, G., Soyer, H.P., Chimenti, S., Talamini, R., Corona, R., Sera, F., Kopf, A.W. (2003). Dermoscopy of pigmented skin lesions: results of a consensus meeting via the Internet. *Journal of the American Academy of Dermatology,* 48(5), 679-93.

[2] Braun, R.P., Rabinovitz, H.S., Krischer, J., Kreusch, J., Oliviero, M, Naldi, L., Saurat, J.H. (2002). Dermoscopy of Pigmented Seborrheic Keratosis: A Morphological Study. *Archives of Dermatology*, 138, 1556-1560.

[3] Cheng, Y., Swamisai, R., Umbaugh, S.E., Moss, R.H., Stoecker, W.V., Teegala, S., Srinivasan, S.K. (2008). Skin lesion classification using relative color features. *Skin Research and Technology*, 14(1), 53-64.

[4] Dalal, A., Moss, R.H., Stanley, R.J., Stoecker, W.V., Gupta, K., Calcara, D.A., Perry, L.A. (2011). Concentric decile segmentation of white and hypopigmented areas in dermoscopy images of skin lesions allows discrimination of malignant melanoma, *Computerized Medical Imaging and Graphics,* 35(2), 148-54.

[5] Gonzalez, R.C. & Woods, R.E. (2002). *Digital Image Processing*. 2nd ed. New Jersey: Prentice Hall, pp. 698-704.

[6] Lee, T.K. (2001). Measuring border irregularity and shape of cutaneous melanocytic lesions. Ph.D. Thesis, Simon Fraser University,Vancouver, British Columbia.

[7] MATLAB version 7.8.0 (R2009a). 2009. Image Processing Toolbox. Natick, Massachusetts: The MathWorks Inc.

[8] Menzies, S.W., Kreusch, J., Byth, K., Pizzichetta, M.A., Marghoob, A., Braun, R., Johr, R. (2008). Dermoscopic evaluation of amelanotic and hypomelanotic melanoma. *Archives of Dermatology,* 144(9), 1120-7.

[9] Stoecker, W.V., Gupta, K., Stanley, R.J., Moss, R.H., & Shrestha, B. (2005_. Detection of asymmetric blotches (asymmetric structureless areas) in dermoscopy images of malignant melanoma using relative color. *Skin Research and Technology,* 11(3), 179-84.

[10] Stricklin, S.M., Stoecker, W.V., Oliviero, M.C., Rabinovitz, H.S., & Mahajan, S.K. (2011). Cloudy and starry milia-like cysts: how well do they distinguish seborrheic keratoses from malignant melanoma? *Journal of the European Academy of Dermatology and Venereology*, 25(10), 1222-4.

III. TWO-STAGE ADAPTABLE TEMPLATE MATCHING FOR DETECTION OF CLOUDY MILIA-LIKE CYSTS IN SKIN LESIONS

Sneha K. Mahajan (SK), Randy H. Moss (RM), Ryan K. Rader (RR), Jason Hagerty (JH), William V. Stoecker (WVS)

ABSTRACT—

Milia-like cysts (MLCs) are dermoscopic structures frequently observed in seborrheic keratoses (SKs), the most common type of skin lesions in older adults. Diversity in SK appearance makes it difficult to differentiate SK from melanoma, which can be deadly. Cloudy MLCs are effective structures in distinguishing SKs from melanoma. This research presents a novel adaptable two-stage correlation model to accurately detect MLCs. Another novel aspect of this research is the use of boundary bands, to record the intensity drop around the entire cloud border to capture the fuzziness of the cloud border. Further analysis is done by extracting various features such as color, shape and intensity drop. The final model generated by stepwise logistic

INDEX TERMS— template matching, melanoma, milia-like cysts, seborrheic keratoses, segmentation

1. INTRODUCTION

Milia-like cysts (MLCs) are small roughly round white to yellowish structures present in “certain pigmented lesions, particularly seborrheic keratoses and congenital melanocytic nevi” [1, 2]. MLCs are classified into two main groups: starry MLCs, generally < 1/3mm, and cloudy MLCs, > 1/3mm (Figure 15) [3]. Starry MLCs appear as “stars on a misty night,” and are found in seborrheic keratoses (SKs), congenital nevi and sometimes in malignant lesions. Cloudy MLCs have fuzzy borders like clouds, vary in shape from circular, oval to irregular shapes and are almost always found in benign lesions (odds ratio for SK/Melanoma = 27.4) [3].

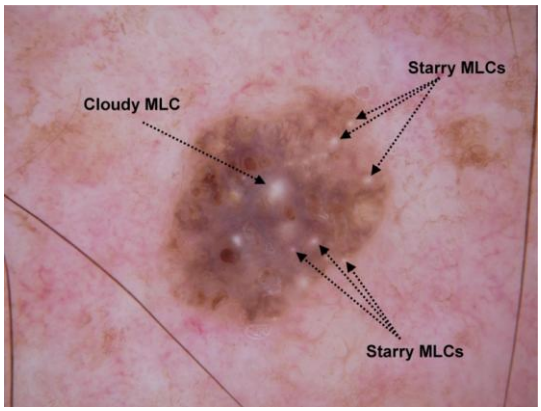

Figure 15: Seborrheic keratosis with a cloudy MLC and multiple starry MLCs. (Stricklin et al.)

A statistical study conducted by Stricklin et al. determined the likelihood of cloudy MLCs appearing in melanomas versus seborrheic keratoses. Cloudy MLCs had an odds ratio of 27.4, 20.0% sensitivity, and 99.1% specificity for seborrheic keratoses versus melanomas [3]. Thus cloudy MLCs can be a strong indicator for dermatologists to suggest that a lesion is not malignant. This paper presents an approach to detect cloudy MLCs to support Stricklin’s hypothesis.

Cloudy MLCs have a distinct appearance in a dermoscopic image of a lesion. Cloudy MLCs within a SK are shown (Figure 16). They are seen to be bright, have a yellowish or whitish coloring and are predominantly oval or roundish in shape, though irregular shapes can be observed. Melanoma images infrequently have similar structures (Figure 17). These mimics are similar in shape, but lighter in color, with clinical observation predicting greater specificity for color than shape for these structures.

Template matching has been used as an important tool to determine locations and or presence of features prior to further detailed analysis in image segmentation. Normalized cross-correlation is the basic method for matching [4]. Normalization allows comparison of features of different structures. This normalized calculation allows independence from overall structure brightness. Dependence upon object size is maintained. The problem with one-stage template matching is the computational intensity

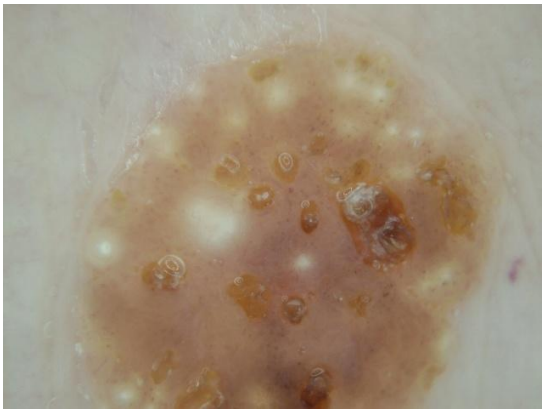

Figure 16: Seborrheic keratosis with multiple cloudy MLCs

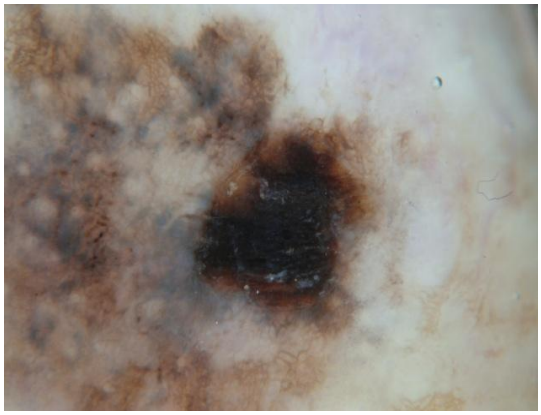

Figure 17: Melanoma showing multiple cloudy MLC mimics.

that results from the large number of computations needed if no prescreening is used. The solution to this problem is a two-stage cross-correlation approach described by Goshtasby [4], used to reduce the number of candidates.

The remainder of this paper includes the following sections: 2) Methods (overview, data sets and pre-processing, 1st stage templates, shape estimation, 2nd stage templates, feature generation and logistic regression methods), 3) Results 4) Discussion and Conclusions.

2. METHODOLOGY OVERVIEW

An overview of the methodology used in this research study is shown in the flowchart in Figure 18. A two-stage template matching approach is used. At the first stage, the image is scanned for MLC candidates, saving candidate locations. The second stage gives a shape estimate for the MLC candidate. This shape is used to generate the adaptive template.

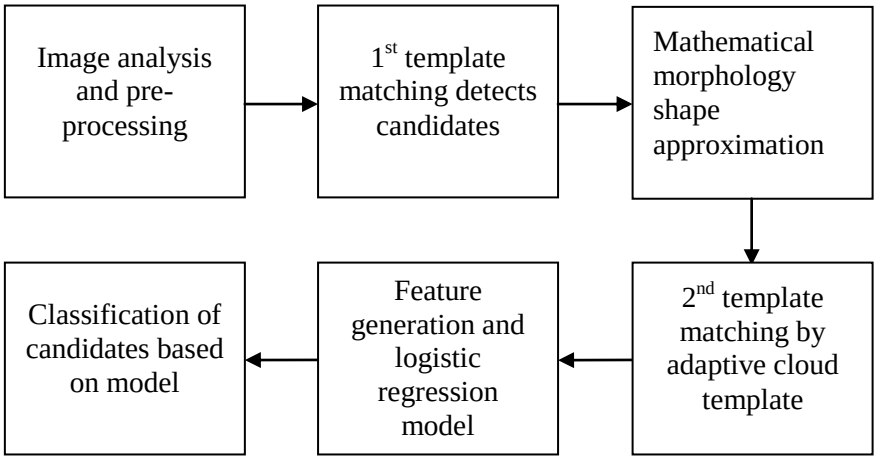

Figure 18: Methodology overview.

Feature generation includes color and shape generation—both features are needed to distinguish cloudy MLCs from mimics in a lesion image. The shape features include normalized cross correlation with a manually created cloud template, normalized cross correlation with an adaptive cloudy MLC template, area of candidates, eccentricity, and solidity. Statistical features such as the variance and standard deviation of cloud area and its surrounding also proved helpful.

2.1 DATA SETS AND PREPROCESSING

This study utilizes two 1024x768 full color sets of contact dermoscopy images. Contact dermoscopy are 10-power images using gel for the device-skin interface. A testing set and a training set each composed of 42 benign seborrheic keratoses and 42 melanomas were used. The training set is used to train the mathematical model to weight each significant feature; the test set is used to validate the model. All images were collected for the study SBIR R44 CA101639-02A2 of the National Institutes of Health (NIH), which was approved by the Phelps County Regional Medical Center Institutional Review Board, Rolla, MO, under the guidelines of the Belmont Report.

Image normalization, determination of manual lesion borders by a dermatologist (WVS) and determination of relative colors (lesion color normalized by skin background color) were the same as described elsewhere [5]. Features for both lesion and regions of interest within the lesion were derived from the red, green and blue (RGB) color space and the hue saturation and value (HSV) color space.

2.2 LEVEL 1 TEMPLATE MATCHING

The first step used fast normalized cross-correlation described mathematically [6]:

$$\gamma(u,v) = \frac{\sum_{x,y}[\,f(x,y)-\bar{f}_{u,v}\,][\,t(x-u,y-v)-\bar{t}\,]}{\{\sum_{x,y}[\,f(x,y)-\bar{f}_{u,v}\,]^2\,\sum_{x,y}[\,t(x-u,y-v)-\bar{t}\,]^2\}^{0.5}} \quad (1)$$

where $\bar{t}$ is the mean of the feature and $\bar{f}_{u,v}$ is the mean of f(x,y) in the region under the feature. The range of γ is -1 to 1, with 1 being a perfect match. This function is implemented by the MATLAB function normxcorr2() [7].

After studying the various cloudy MLCs among the lesions in the training set, it is observed that the average size of a cloudy MLC would be of a radius in the range of about 25 to 40 pixels. It was found that a radius of 30 pixels was the best estimate. This range is used to make a generalized template in the form of a disk with fuzzy borders, which will be used as a quick initial filter to mark the likely candidates. The cloud template used in this step was generated by using a 61x61 Gaussian kernel with $\sigma = 25$ (Figure 19).

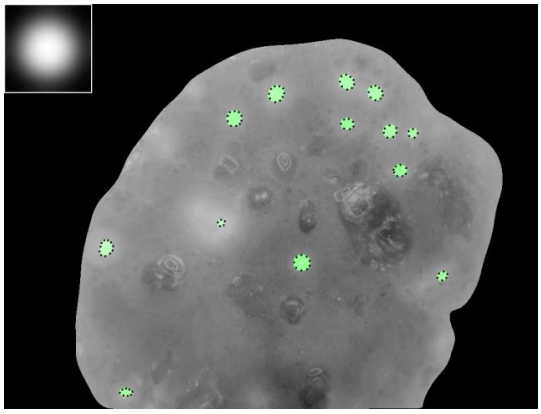

Figure 19: Candidates marked at level 1 template matching

This gives us a template of desired radius ~30. The value of σ determines the desired fuzziness and spread of the disk. This template along with the lesion image is used in the MATLAB function normxcorr2() and the result is a grayscale intensity image, in the range -1 to 1, with highest average values in areas of high possibility of cloudy MLC presence. Cloudy MLC candidate pixels with $\gamma \leq 0.65$ are discarded. At this point, passing candidates contain 90.4% of all true cloudy MLCs present, (9.6% of cloudy MLCs are discarded) as well as cloudy MLC mimics numbering 160% of the true cloudy MLCs (Figure 19).

Figure 19 shows the image as a result of this initial filtering process. Candidates passing first-stage template matching areas are overlaid with green disks with dotted edges. The disk radii are proportional to γ. Each blob with disk overlay passed the $\gamma >$ 0.65 threshold. After the first stage, no color information or details of shape information about passing MLCs is known, and a second stage is necessary. The centroids of the blobs detected in this step are used as starting points for additional examination. The next step in making a deduction is the shape estimation for the candidate.

2.3 SHAPE ESTIMATION VIA MORPHOLOGICAL TECHNIQUES

To systematically approximate the size and shape variation exhibited by a typical cloudy MLC, several ideal static templates for circular and oval MLCs were used for cross-correlation. These templates did not capture the variable shape and size of MLCs. An adaptive method to correctly estimate this shape and size along with preserving the necessary features such as fuzziness of borders and peaks was required. Thus grayscale morphological reconstruction techniques called "opening-by-reconstruction" and "closing-by-reconstruction" were used for shape estimation [8]. This technique marks the flat regional maxima and minima in the image, while preserving the original shape of the cloudy MLCs. Opening and closing by reconstruction requires two inputs, a marker which contains the starting points for the transformation and a mask which imposes a constraint on the transformation [8].

"Opening by reconstruction" of size n of a gray-scale image f is reconstruction by dilation of f from the erosion of size n of an input image by a structuring element, the result of this operation is then used as a marker for its morphological reconstruction [8]. n indicates the number of times an operation is performed.

$$O_R^{(n)}(f) = R_f^D[(f \ominus nb)] \quad (2)$$

where $(f \ominus nb)$ denotes n erosions of f by b. In our case, f denotes the lesion image, b denotes a structuring element of a disk of radius 15 pixels and n=1. R_f^D denotes reconstruction by dilation operation on f. $O_R^{(n)}$ denotes the resulting image shown in Figure 20b, which will be used as the mask for the closing by reconstruction operation. This operation has a leveling effect on the bright areas of the image. As observed, the bright areas and their shapes are highlighted.

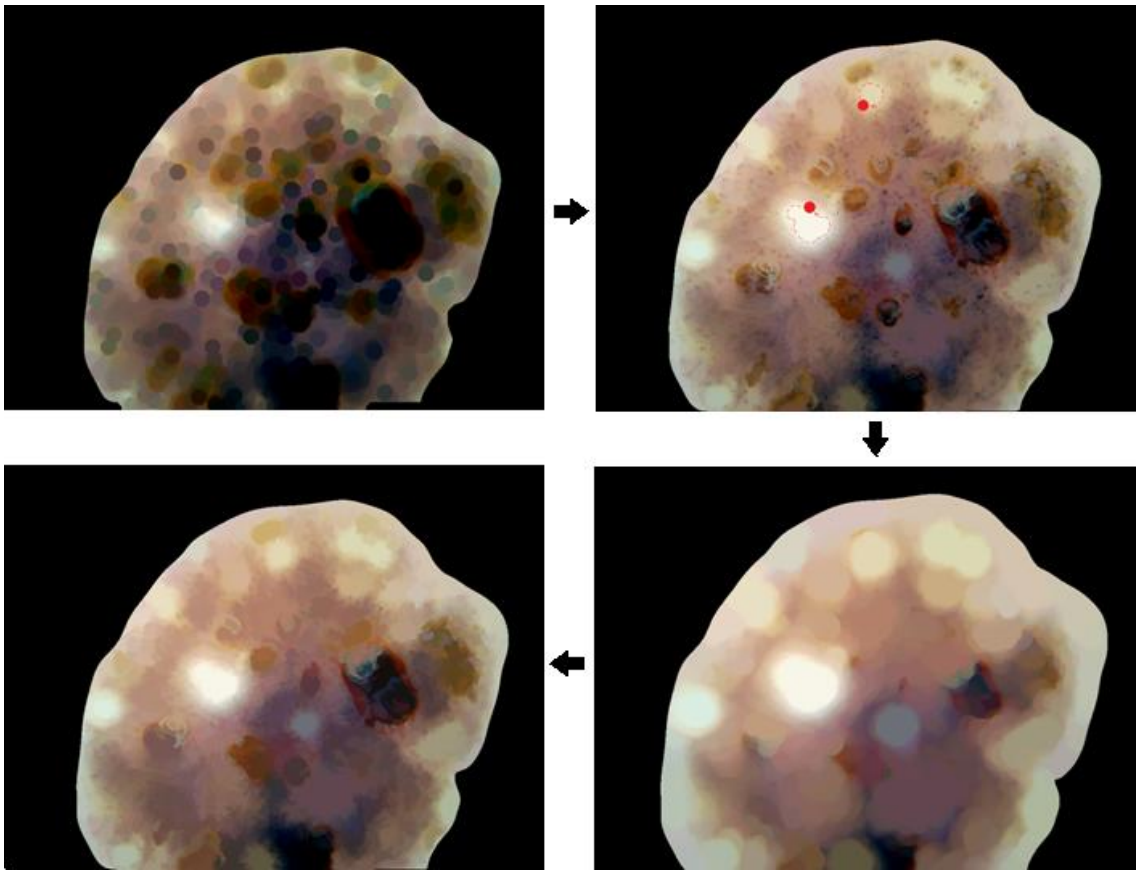

Figure 20: Grayscale reconstruction process. a) Erosion by 15x15 disk structuring element. b) First reconstruction operation with 2 dilation structuring elements and resultant objects. c) Dilation by 15x15 disk structuring element. d) Second reconstruction operation

"Closing by reconstruction" is reconstruction by erosion of f after dilation of size n followed by its morphological reconstruction [8].

$$C_R^{(n)}(f) = R_f^E[(f \oplus nb)] \tag{3}$$

where $(f \oplus nb)$ denotes n dilations of f by b. R_f^E denotes reconstruction by erosion of f. In our case, f denotes $O_R^{(n)}$ and b denotes a structuring element of 15 x 15 disk and n=1. $C_R^{(n)}$ denotes the resulting image shown in Figure 20d, which will be used to create binary masks for cloud areas. This operation suppresses small stray noisy blobs, giving a leveling effect on the dark areas in the image. It is now possible to approximate cloud shape, since all pixels in a given cloud now have a level value. In the section ahead, these extracted shapes will be used to create templates for individual clouds.

2.4 ADAPTABLE CLOUD TEMPLATE FORMATION

An irregular cloud template corresponding to every individual candidate is created. The purpose of this is to have a better estimate of shape while the color and statistical features are extracted. Cloud shapes are directly derived from the intensity image of Figure 20d. To mark each blob in this image a method called region growing is used, where a region at the point of use is grown by comparing all unallocated neighborhood pixels in its surrounding to the allocated region [9]. The difference between a pixel intensity value and the regions mean is used as a decision measure. The process stops when the difference becomes larger than the threshold. This code is developed by Dirk-Jan Kroon [9]. The points of interest in this case are the centroids of the green blobs in Figure 19. A binary image is obtained as a result of this operation and

is shown in Figure. 21. The blobs in this image are a much better estimate of shape for the clouds as compared to the blobs in Figure 19.

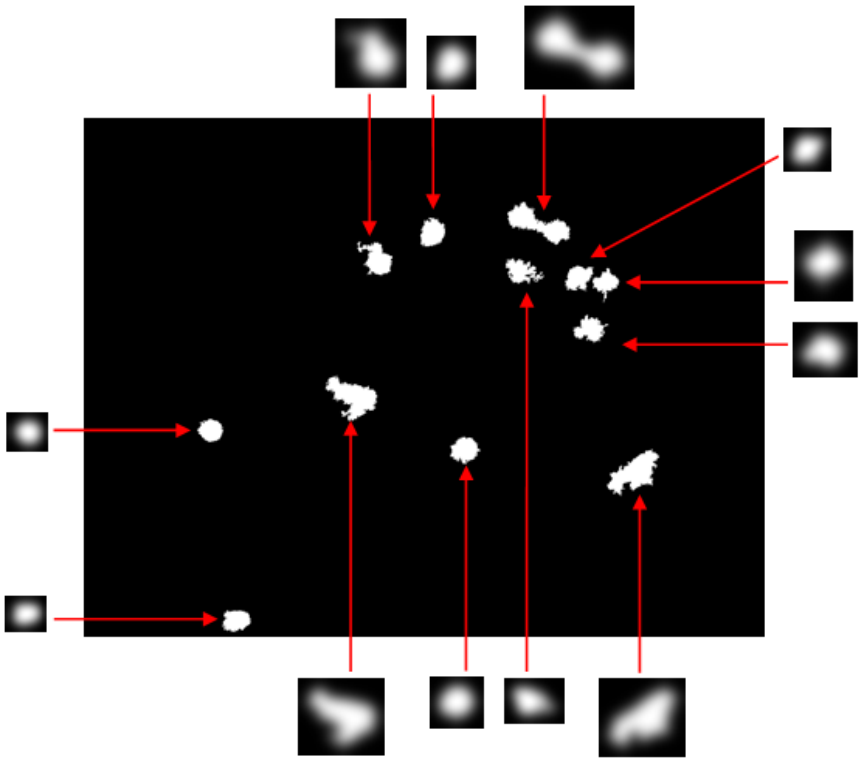

Figure 21: Adaptive cloud templates

Each blob in this binary image will be used to create a template for the respective cloud, using a Gaussian kernel with σ=25 constrained by shape and size of the individual blob. This operation has a spreading effect on the binary image. Figure 21 shows the irregular cloud templates created corresponding to its blob. This process will be done for each image and each blob. In the next sections, the blobs obtained in this section will serve as masks for various features for that particular image. This step is performed individually for each blob extracted from each lesion image.

2.5 FEATURE GENERATION

All features (Table 2) are recorded for each blob location that is marked at the level 1 template matching for the 42 benign and 42 malignant images. All features are

Table 2: Features extracted from blobs

Features	Equations
Average grayscale	**A=(R+G+B) / 3**
Absolute RGB	**Absolute R = Red Average over cloud mask** **Absolute G = Green Average over cloud mask** **Absolute B = Blue Average over cloud mask**
Relative RGB	**Relative R = Absolute R - Skin R** **Relative G = Absolute G - Skin G** **Relative B = Absolute B - Skin B**
RGB Chromaticity	**R Chromaticity = R / (R+G+B)** **G Chromaticity = G / (R+G+B)** **B Chromaticity = B / (R+G+B)**
Relative RGB Chromaticity	**Relative R Chromaticity = Relative R / Relative(R+G+B)** **Relative G Chromaticity = Relative G / Relative(R+G+B)** **Relative B Chromaticity = Relative B / Relative(R+G+B)**
Converting RGB color plane to HSV color plane [10]	**V = [max(R, G, B)] and X=[min(R, G, B)]** **S =** $\begin{cases} \frac{V-X}{V} \end{cases}$; $if\ S = 0\ return;$ **r =** $\frac{V-R}{V-X}$, **g =** $\frac{V-G}{V-X}$, **b =** $\frac{V-B}{V-X}$ $if\ R = V\ then\ H = (if\ G = X\ then\ 5 + b\ else\ 1 - g)$ $if\ G = V\ then\ H = (if\ B = X\ then\ 1 + r\ else\ 3 - b)$ $else\ H = (if\ R = X\ then\ 3 + g\ else\ 5 - r)$
Maximum cross-correlation coefficient of blob	**max{** $\gamma(u, v)$ **} for area over cloud mask**

Table 3: Features extracted from blobs (contd.)

Standard deviation	$\left\{\frac{1}{n}\sum_{x,y}[\,f(x,y)-\bar{f}\,]^2\right\}^{\frac{1}{2}}$ **where f is area under mask** **$\bar{f}$ is mean of area under mask** **n is number of pixels in area**
Average cross-correlation coefficient of blob	**avg{ $\gamma(u,v)$} for area over cloud mask**
Adaptive cross-correlation coefficient	**Cross-correlation coefficient calculated using adaptable cloud template**
Boundary bands for blob	**In Figure 22, the area 5 has thickness 4 pixels and is centered on the boundary of the blob and grey level areas 1, 2, 3, and 4 show the areas of thickness 4 pixels moving out from the boundary and the areas 6, 7, 8, and 9 indicate areas of thickness 4 moving in from the boundary. Intensity drops are differences between average intensity values over these sequential areas. For example, intensity drop at 4 = (average intensity at 5 – average intensity at 4)**
Blue chromaticity image	**This is the 1024x768 image of blue chromaticity ($B_{x,y}$ / ($R_{x,y}$+$G_{x,y}$+$B_{x,y}$) calculated at each pixel. Average blue chromaticity is calculated in an area surrounding the cloud mask which is 2 times the area of the cloud mask. Blue chromaticity variance = (Variance of blue chromaticity image calculated in the same area surrounding the cloud mask)**

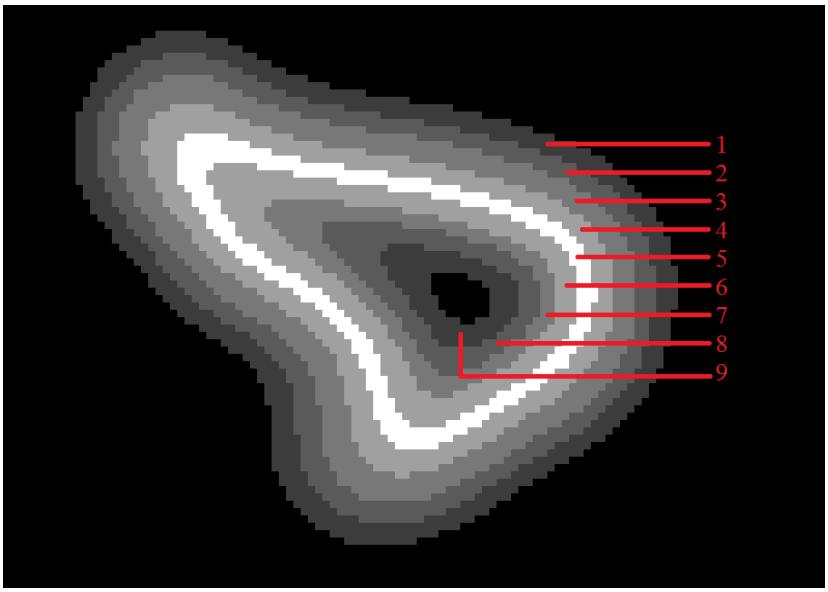

Figure 22: Boundary bands calculated over areas 6, 7, 8, and 9 moving inwards from white boundary and over 1, 2, 3, and 4 moving outwards from white boundary.

calculated for the blob mask and for surround features, for an area of 15 pixels surrounding the blob. The training step was used to manually mark all cloudy MLCs after the first stage template. Stepwise logistic regression (Proc Logistic, SAS Inc., Cary, NC) was implemented to determine the significant features, using a significance level of 50% (SLEntry=0.50 in SAS) for the feature to enter the model and a significance level of 95% (SLStay=0.05 in SAS) for the feature to stay in the model.

3. RESULTS

A total of 62 features were analyzed among which seven features were selected as significant by the logistic regression model at a SLEntry = 0.50 and SLStay = 0.05. The significant features are listed in Table II. The receiver operating characteristic (ROC) curve, the plot of sensitivity vs. 1-specificity is shown (Figure 23). The Proc Logistic c statistic = 0.924 gives an estimate for the area under the ROC curve which can also be observed in Figure 23. A model that is able to accurately distinguish between benign SKs and melanomas using cloudy MLCs and their mimics is more desirable as opposed to a model which identifies all cloudy MLCs. Thus we want the model to have a higher specificity.

The results were confirmed by applying the model on an independent test set of 42 benign and 42 melanoma images. The accuracy measured was based on each candidate being identified correctly. A specificity of 95.78% (in 166 candidates only 7 were falsely classified as mimics) for false negatives and 61.76% sensitivity (for 63/102) for cloudy MLCs was observed.

4. DISCUSSION AND CONCLUSIONS

This paper examines different approaches to automatically detect and segment a cloudy MLC in a given dermoscopic image of a skin lesion and supports the hypothesis presented by Stricklin et. al [3]. To mark the location of MLCs a hierarchical template matching approach is followed. In Table II., a ChiSq value less than 0.001, corresponding to a feature indicates that the feature is significant in distinguishing the MLCs from competitive structures in melanomas such as hypo-pigmented round and fuzzy skin networks. Thus, average absolute red over cloud mask, green chromaticity over cloud mask, green chromaticity around cloud, maximum correlation of the MLCs and variance in blue chromaticity are the most significant features. Also, the 'Estimate' column indicates the weight for these parameters in the model. The accuracy and area under the ROC curve show that the model presented in this paper can identify true cloudy MLCs from mimics with a precision of 84.8%. The results from the test set validate this model.

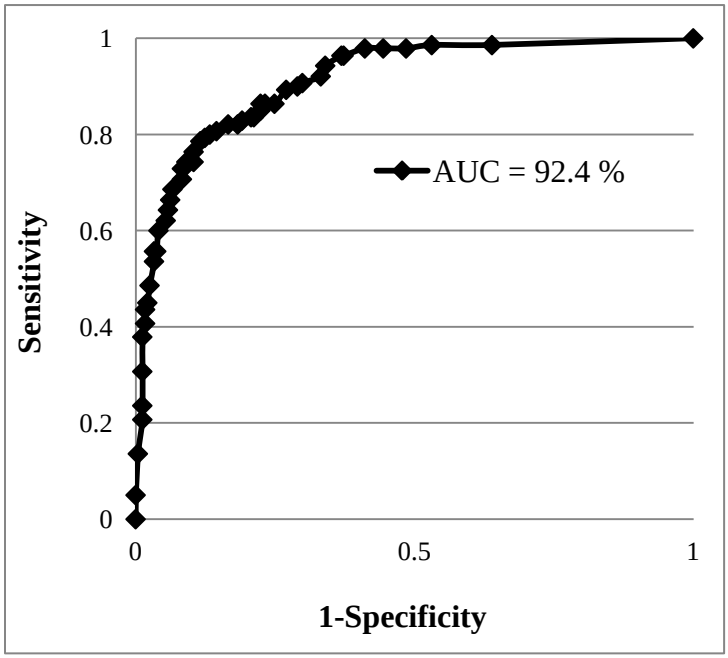

Figure 23: Receiver Operating Characteristics showing AUC

With the current training set of 84 images, the number of candidates per image in the melanomas was not more than 3. Testing the model on the test set showed better results with not more than 1 false positive per image in the melanomas. This number is likely to vary between 1- 4 per image based on the size of training set used. In conclusion, this model can be successfully used as a method to classify a lesion as benign based on the number of cloudy MLCs. For example, a dermoscopic image of a skin lesion containing 4 or more MLCs could be diagnosed as benign. Further improvements include using a training set with a larger variety of cloudy MLCs, where variety refers to size, shape, color and intensity. This will enable the model to capture the immense variation that is very typical to a cloudy MLC.

Computational complexity of the algorithm for shape estimation via morphological techniques was high. On a 1.3 GHz, Windows 7, 64 bit operating system with a RAM of 4 GB the program needed 20 minutes to process 84 images without the shape estimation and 60 minutes with it. Using faster algorithms for image reconstruction could help. This model can also be integrated with the model for detecting starry milia-like cysts presented by Subramanian [11]. Considering the presence of both starry and cloudy MLCs in a lesion might improve accuracy of diagnosis.

Table 4: Analysis of Maximum Likelihood Estimates

Parameter	DF	Estimate	Standard Error	Wald Chi-Square	Pr > ChiSq
Intercept	**1**	**-46.2983**	**6.8746**	**45.3561**	**<.0001**
Average absolute red over cloud mask	**1**	**-4.6999**	**1.0888**	**18.633**	**<.0001**
Green chromaticity over cloud mask	**1**	**480.7**	**72.1825**	**44.3495**	**<.0001**
Green chromaticity around cloud mask	**1**	**-362.2**	**60.67**	**35.6472**	**<.0001**
Hue surrounding cloud mask	**1**	**-3.6608**	**1.5531**	**5.556**	**0.0184**
Maximum correlation over cloud mask	**1**	**12.2697**	**2.5637**	**22.9048**	**<.0001**
Blue chromaticity variance	**1**	**-10986.3**	**2148.5**	**26.1468**	**<.0001**
Average blue chromaticity	**1**	**4.5305**	**1.7333**	**6.8321**	**0.009**

REFERENCES

[1] D.R. Berk, S.J. Bayliss, "Milia: a review and classification," *J. Am. Acad. Dermatol.,* vol. 59, pp. 1050-1063, Dec. 2008.

[2] G. Argenziano, H.P. Soyer, S. Chimenti, et al., "Dermoscopy of pigmented skin lesions: results of a consensus meeting via the internet," *J. Am. Acad. Dermatol.,* vol. 48, pp. 679-93, May 2003.

[3] S.M. Stricklin, W.V. Stoecker, M.C. Oliviero, et al., "Cloudy and starry milia-like cysts: how well do they distinguish seborrheic keratoses from malignant melanomas?" *J. Eur. Acad. Dermatol. Venereol.,* vol. 25, no. 10, pp. 1222-4, Oct. 2011.

[4] A. Goshtasby, S. H. Gage, and J. F. Bartholic, "A Two-Stage Cross Correlation Approach to Template Matching ," IEEE Trans. Pattern Analysis and Machine Intelligence, vol. 6, no. 3, pp. 374-378, May 1984.

[5] M.E. Celebi, G. Schaefer, H. Iyatomi, et al., "An improved objective evaluation measure for border detection in dermoscopy images," *Skin Res. Technol.,* vol. 15, pp. 444-450, Nov. 2009.

[6] J. P. Lewis, "Fast Template Matching," *Vision Interface,* p. 120-123, May 1995.

[7] MATLAB version 7.8.0 (R2009a). 2009. Image Processing Toolbox. Natick, Massachusetts: The MathWorks Inc.

[8] R.C. Gonzalez & R.E. Woods, *Digital Image Processing,* 2nd ed., New Jersey: Prentice Hall, 2002.

[9] D.-J. Kroon, Region Growing [Computer program]. Available at http://www.mathworks.com/matlabcentral/fileexchange/19084-region-growing (Accessed 18 September 2012)

[10] A. R. Smith, "Color Gamut Transform Pairs," In *SIGGRAPH 78 Conf. Proc.*, pp. 12-19, Aug 1978.

[11] V. Subramanian, R.H. Moss, R.K. Rader, S.K. Mahajan, W.V. Stoecker, "Template Matching for Detection of Starry Milia-like Cysts in Dermoscopic Images (Accepted for publication)," In *International Conference on Computer Vision Theory and Applications (VISAPP)*, to be published.

[12] R. P. Braun, H. S. Rabinovitz, M. Oliviero, A. W. Kopf, and J.-H. Saurat, "Dermoscopy of pigmented skin lesions," *J. Am. Acad. Dermatol.,* vol. 52, pp. 109-121, Jan. 2005.

[13] S. W. Hermansen, "Evaluating Predictive Models: Computing and Interpreting the c Statistic," Paper 143-2008, SAS Global Forum 2008.

SECTION

2. CONCLUSIONS

This research studies the importance of dermoscopic structures called milia-like cysts in distinguishing seborrheic keratoses from malignant melanoma lesions. The presence of the both cloudy and starry MLCs is analyzed, with specificity for seborrheic keratoses in the presence of cloudy MLCs being higher (99.1 %). Thus, detection of cloudy milia-like cysts can be a more helpful sign for dermatologists to diagnose a lesion as benign. The model presented in "Two-Stage Adaptable Template Matching for Detection of Cloudy Milia-like Cysts in Skin Lesions," detects a cloudy MLC in a skin lesion with an accuracy of 84.8 %. The model is validated with a test set and no more than one mimic per image is detected. This number is likely to vary based on the training set from1-4 and can be used as a measure to diagnose a lesion as benign. For example, a lesion with more than four cloudy MLCs can be diagnosed as benign.

VITA

Sneha Mahajan was born in Nashik, India on the 14th of May, 1988. She received her primary and secondary education from St. Philomena's Convent High School in Nashik, Maharashtra, India. She completed her secondary education in May 2003 and then joined the R. Y. K. college of Arts and Science, Nashik in the science stream. She graduated with a Bachelor of Engineering degree in Electronics and Telecommunication from K. K. Wagh College of Engineering, Nashik in May 2009.

She enrolled as a graduate student in Missouri University of Science and Technology, Rolla, MO in January 2010, majoring in Electrical Engineering. She was a Graduate Research Assistant in the DERMVIS group of cancer research from May 2010 to December 2012 and received her MS degree in Electrical Engineering in May 2013.